

Enhancing the thermoelectric performance through the mutual interaction between conjugated polyelectrolytes and single-walled carbon nanotubes

Shuxun Wan(万树勋), Zhongming Chen(陈忠明), Liping Hao(郝丽苹), Shichao Wang(王世超), Benzhang Li(李本章), Xiao Li(黎潇), Chengjun Pan(潘成军), and Lei Wang(王雷)

Citation: Chin. Phys. B, 2022, 31 (**2**): 028104. DOI: 10.1088/1674-1056/ac48f9
Journal homepage: http://cpb.iphy.ac.cn; http://iopscience.iop.org/cpb

What follows is a list of articles you may be interested in

Thermoelectric characteristics of flexible reduced graphene oxide/silver selenide nanowire composites prepared by a facile vacuum filtration process

Zuo Xiao(肖佐), Yong Du(杜永) , Qiufeng Meng(孟秋风) , and Lei Wang(王磊)
Chin. Phys. B, 2022, 31 (**2**): 028103. DOI: 10.1088/1674-1056/ac447e

Silica encapsulated ZnO quantum dot-phosphor nanocomposites: Sol-gel preparation and white light-emitting device application

Ya-Chuan Liang(梁亚川), Kai-Kai Liu(刘凯凯), Ying-Jie Lu(卢英杰), Qi Zhao(赵琪), Chong-Xin Shan(单崇新)
Chin. Phys. B, 2018, 27 (**7**): 078102. DOI: 10.1088/1674-1056/27/7/078102

In situ growth of different numbers of gold nanoparticles on MoS_2 with enhanced electrocatalytic activity for hydrogen evolution reaction

Xuan Zhao(赵宣), Da-Wei He(何大伟), Yong-Sheng Wang(王永生), Chen Fu(付晨)
Chin. Phys. B, 2018, 27 (**6**): 068103. DOI: 10.1088/1674-1056/27/6/068103

Phase transition of a diblock copolymer and homopolymer hybrid system induced by different properties of nanorods

Xiao-bo Geng(耿晓波), Jun-xing Pan(潘俊星), Jin-jun Zhang(张进军), Min-na Sun(孙敏娜), Jian-yong Cen(岑建勇)
Chin. Phys. B, 2018, 27 (**5**): 058102. DOI: 10.1088/1674-1056/27/5/058102

High thermal stability of diamond-cBN-B_4C-Si composites

Hong-Sheng Jia(贾洪声), Pin-Wen Zhu(朱品文), Hao Ye(叶灏), Bin Zuo(左斌), Yuan-Long E(鄂元龙), Shi-Chong Xu(徐仕翀), Ji Li(李季), Hai-Bo Li(李海波), Xiao-Peng Jia(贾晓鹏), Hong-An Ma(马红安)
Chin. Phys. B, 2017, 26 (**1**): 018102. DOI: 10.1088/1674-1056/26/1/018102

SPECIAL TOPIC — Organic and hybrid thermoelectrics

Enhancing the thermoelectric performance through the mutual interaction between conjugated polyelectrolytes and single-walled carbon nanotubes

Shuxun Wan(万树勋)[1], Zhongming Chen(陈忠明)[2], Liping Hao(郝丽苹)[1], Shichao Wang(王世超)[1], Benzhang Li(李本章)[1], Xiao Li(黎潇)[1], Chengjun Pan(潘成军)[1,‡], and Lei Wang(王雷)[1,†]

[1] *Shenzhen Key Laboratory of Polymer Science and Technology, College of Materials Science and Engineering, Shenzhen University, Shenzhen* 518060, *China*
[2] *School of Environment and Civil Engineering, Dongguan Cleaner Production Technology Centre, Dongguan University of Technology, Dongguan* 523808, *China*

(Received 31 July 2021; revised manuscript received 2 January 2022; accepted manuscript online 7 January 2022)

We present a method of constructing composites composed of conjugated polyelectrolytes (CPEs) and single-walled carbon nanotubes (SWCNTs) to obtain a high-performing flexible thermoelectric generator. In this approach, three kinds of polymers, namely, poly[(1,4-(2,5-didodecyloxybenzene)-alt-2,5-thiophene] (P1), poly[(1,4-(2,5-bis-sodium butoxysulfonate-phenylene)-alt-2,5-thiophene] (P2), and poly[(1,4-(2,5-bis-acid butoxysulfonic-phenylene)-alt-2,5-thiophene] (P3) are designed, synthesized and complexed with SWCNTs as thermoelectric composites. The electrical conductivities of the CPEs/SWCNTs (P2/SWCNTs, and P3/SWCNTs) nanocomposites are much higher than those of non-CPEs/SWCNTs (P1/SWCNTs) nanocomposites. Among them, the electrical conductivity of P2/SWCNTs with a ratio of 1:4 reaches 3686 S·cm^{-1}, which is 12.4 times that of P1/SWCNTs at the same SWCNT mass ratio. Moreover, CPEs/SWCNTs composites (P2/SWCNTs) display remarkably improved thermoelectric properties with the highest power factor (PF) of 163 μW·m^{-1}·K^{-2}. In addition, a thermoelectric generator is fabricated with P2/SWCNTs composite films, and the output power and power density of this generator reach 1.37 μW and 1.4 W·m^{-2} (cross-section) at $\Delta T = 70$ K. This result is over three times that of the thermoelectric generator composed of non-CPEs/SWCNTs composite films (P1/SWCNTs, 0.37 μW). The remarkably improved electrical conductivities and thermoelectric properties of the CPEs/SWCNTs composites (P2/SWCNTs) are attributed to the enhanced interaction. This method for constructing CPEs/SWCNTs composites can be applied to produce thermoelectric materials and devices.

Keywords: composites, thermoelectric, SWCNTs, conjugated polyelectrolytes

PACS: 81.05.Qk, 72.15.Jf, 81.05.U−, 81.05.Lg **DOI:** 10.1088/1674-1056/ac48f9

1. Introduction

Many researchers have focused on thermoelectric materials, which are able to implement the conversion between thermal energy and electrical energy based on the Seebeck effect, due to their critical role in renewable energy utilization and solving the energy crisis. Thermoelectric materials possess good application prospects for sustainable technologies.[1,2] However, they exhibit a major problem in that the thermoelectric conversion efficiency is low, which hinders their development. The thermoelectric material conversion efficiency can be assessed through the thermoelectric figure ZT, represented by $ZT = TS^2\sigma/\kappa$ (T is the absolute temperature, S is the Seebeck coefficient, σ is the electrical conductivity, and κ is the thermal conductivity). For most organic materials, the power factor (PF $= S^2\sigma$) is usually used as a criterion to assess the thermoelectric properties, because the thermal conductivity is low.[3] Conductive polymers have many merits, such as good processability, inexpensiveness, and excellent flexibility, which are applicable for the formulation of flexible thermoelectric devices.[4,5] However, compared with the power factor of inorganic thermoelectric materials, that of conducting polymers is much lower.[4] A feasible method is used to enhance the power factor of conducting polymers through the manufacturing of conducting polymer/inorganic composites by an appropriate strategy.[6–9]

Single-walled carbon nanotubes (SWCNTs) are outstanding materials for developing flexible thermoelectric materials, due to their considerable chemical stability, high conductivity, and mechanical flexibility. Constructing nanocomposites composed of conducting polymers as the matrix and SWCNTs as the fillers has become a common method to enhance the thermoelectric performance of materials.[10] Thus, many researchers are committed to developing nanocomposites composed of conducting polymers and SWCNTs, which lead to a high thermoelectric performance and high conductivity.[11,12]

However, there are few reports on CPEs/SWCNTs composite thermoelectric materials. CPEs are described as conjugated conducting polymers bearing ionic side chains.[13] Mai and Bazan presented some reports about the thermoelectric

†Corresponding author. E-mail: wl@szu.edu.cn
‡Corresponding author. E-mail: pancj@szu.edu.cn

© 2022 Chinese Physical Society and IOP Publishing Ltd

performance of self-doped CPEs and studied the influence of different counterions on the thermoelectric performance.[14] They also found that introducing hydrophilic tetraethylene glycol as side chains can affect the polarization of counterions, which may promote the carrier concentration, followed by the conductivity.[15] In addition, they also proposed that the SWCNTs could be doped by CPEs selectivity to bring about p-type or n-type composites by introducing different pendant ionic functionalities.[16] Some researchers also found that CPEs not only provided interactions between the CPEs and π-framework of the SWCNTs walls but also rendered the CPEs/SWCNTs composites compatible in polar solvents because of the resulting ionic functionalities.[17] Considering many advantages of CPEs that are summarized above, we construct composites composed of CPEs and SWCNTs, and study the influence of the interaction between CPEs and SWCNTs on the thermoelectric properties of the composite films.

Herein, we synthesize three conjugated polymers: poly[(1,4-(2,5-didodecyloxybenzene)-alt-2,5-thiophene] (P1), poly[(1,4-(2,5-bis-sodium butoxysulfonate-phenylene)-alt-2,5-thiophene] (P2), and poly[(1,4-(2,5-bis-acid butoxysulfonic-phenylene)-alt-2,5-thiophene] (P3). Although their conjugated skeletons are the same, the side chains are different. Among them, P1 is non-CPEs, P2 and P3 are CPEs. These three polymers give us a great chance to explore the interaction between CPEs and SWCNTs and its impact on a composite film's thermoelectric performance. Moreover, we combine three polymers with SWCNTs to prepare the P1/SWCNT, P2/SWCNT and P3/SWCNT composites with different SWCNT contents. The influence of the ionic functionalities of the CPEs on the interaction between the polymers and SWCNTs and subsequent impact on thermoelectric performance have been methodically studied. The Raman spectroscopies and ultraviolet-visible (UV–vis) results demonstrate that CPEs have a stronger interaction with SWCNTs than non-CPEs do. The elevated interaction increases the power factor of the P2/SWCNTs hybrid film at a ratio of 1:4 to 163 $\mu W \cdot m^{-1} \cdot K^{-2}$ at room temperature, which is much higher than that of P1/SWCNTs hybrid film (112 $\mu W \cdot m^{-1} \cdot K^{-2}$).

2. Results and discussion

2.1. Materials synthesis

The synthesis routes of P1, P2, and P3 are shown in Scheme S1(a). P1 is obtained by the typical Stille coupling reaction, and P2 is obtained by the Suzuki coupling reaction. The ion exchange of P2 with sulfuric acid provides P3, as shown in Fig. S9, and sodium ions are successfully partially exchanged. All three polymers are well characterized by ^{1}H NMR spectroscopy (Figs. S3–S5), and P1 and P2 are characterized by gel permeation chromatography (GPC) analysis (Fig. S6).

2.2. Study of the photophysical and electrochemical properties of polymers

The absorption spectra of the film and solution states of the polymers are measured through UV–vis absorbance spectroscopy, which are applied to assess the π-electronic structure. The solution and film of P1 are prepared by employing chlorobenzene as the solvent, and the solutions and films of P2 and P3 are prepared by employing water. As illustrated in Figs. 1(a)–1(c), these absorption spectra exhibit a strong absorption band in the wavelength range < 800 nm, and the absorption peak originates mostly from the π–π^* transition of the benzene–thiophene backbone. Moreover, the two

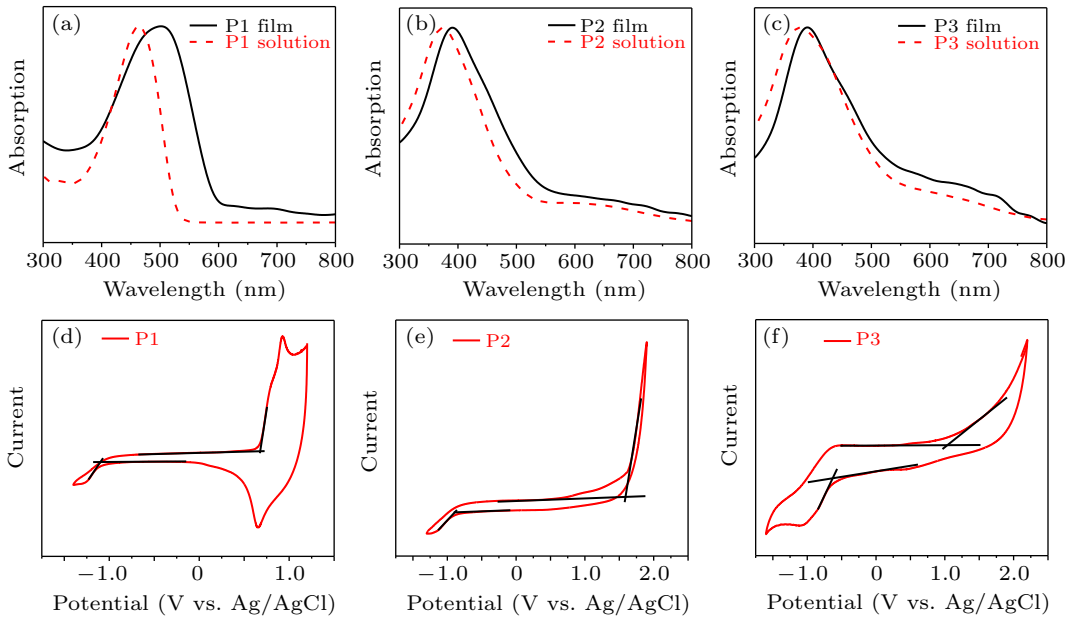


Fig. 1. (a)–(c) UV–vis spectra of P1 in chlorobenzene and P2, and P3 in water solutions and in film states, (d)–(f) CV curves of the polymers.

polyelectrolytes P2 and P3 in solution show maximum absorption at 374 nm and 377 nm, respectively, which are blueshifted relative to P1 (463 nm). Compared to the solution, there is an evident redshift of the absorption maximum band in the film state, owing to the conjugated main chain of the polymer undergoing enforced planarization during the film-forming process.[11]

The electrochemical properties of P1, P2, and P3 are investigated through cyclic voltammetry (CV). The CV curves are displayed in Figs. 1(d)–1(f). In all the polymers' positive potential ranges, there are a couple of reversible redox peaks. The onset oxidation potentials (φ_{ox}) of P1, P2, and P3 are approximately 1.2 V, 1.6 V, and 1.0 V, respectively. The initial oxidation potential is usually interpreted as the point at which the current begins to rise from the baseline.[18] In addition, the onset reduction potentials (φ_{red}) of the P1, P2, and P3 polymers are −1.1 V, −0.89 V, and −0.64 V, respectively. The HOMO energy level represents the ionization energy of a polymer, the P3 polymer shows the shallowest HOMO level among the three polymers, indicating that P3 can be easily doped by same dopants. Moreover, the P3 shows a relatively narrower electrochemical band gap (Table S1).

2.3. Nanocomposite film morphologies

To further study the relationship between the nanostructure morphology, scanning electron microscopy (SEM) is applied to observe the surface morphology of the three composites. SEM images of the P2/SWCNTs nanocomposites with different SWCNT contents are presented in Fig. 2. Moreover, SEM images of the P1/SWCNTs and P3/SWCNTs nanocomposites are shown in Figs. S7 and S8. As presented in Fig. 2(a), the surface topography of polymer P2 is smooth and closely packed, while the SEM images of the P2/SWCNT hybrid films (Figs. 2(b)–2(f)) illustrate that the SWCNTs are evenly dispersed in the nanocomposites. Moreover, there is no apparent cluster phenomenon in the SEM images, indicating that the SWCNTs are well-connected with the CPEs owing to strong π–π interfacial interactions. As a result, a three-dimensional conductive network is obtained. The diameter of the carbon nanotubes increases with increasing SWCNTs content, but the number of three-dimensional conductive networks also increases. The conductivity of the original polymer is far poorer than that of the SWCNTs beam, and the SWCNTs mixture can greatly improve the nanocomposites conductivity. Compared to the P2/SWCNTs composite films, P1/SWCNTs exhibits some clustering phenomena and a larger diameter distribution (Fig. S7), which could impede the formation of three-dimensional conductive networks.[19] P2/SWCNTs nanocomposites exhibit more favourable SWCNTs dispersions than P1/SWCNTs nanocomposites, probably because the interaction between the CPEs and SWCNTs is stronger.

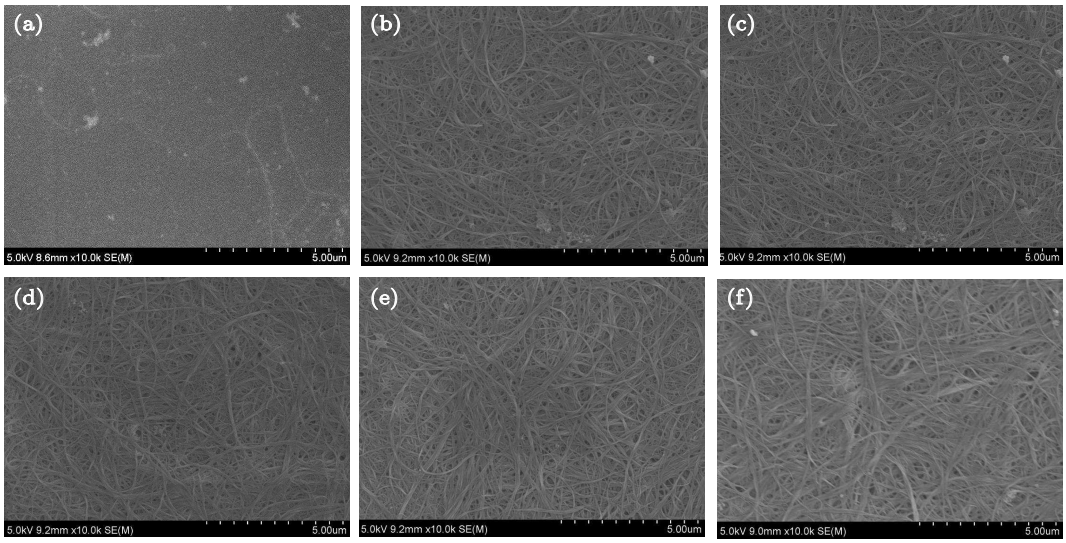


Fig. 2. SEM images of the P2/SWCNT nanocomposite films with mass ratios of (a) 1:0, (b) 4:1, (c) 2:1, (d) 1:1, (e) 1:2, and (f) 1:4.

2.4. Analysis of nanocomposite film photophysical properties

To investigate the interaction between SWCNTs and polymers, the UV-vis absorption spectra of the original SWCNTs and nanocomposite films with different SWCNT contents are measured. As illustrated in Fig. 3, the spectra of the P1/SWCNT, P2/SWCNT, and P3/SWCNT composite films show clear absorption bands at 495 nm, 390 nm, and 389 nm, which originate from the feature absorption bands of P1, P2, and P3 in the nanocomposites. With decreasing polymer loading, the intensities of these peaks gradually decrease, as expected. In addition, pristine SWCNTs show an absorption peak at approximately 291 nm, which is characteristic of SWCNTs.[20] The P1/SWCNTs, P2/SWCNTs, and P3/SWCNTs nanocomposites with 80 wt% SWCNT loading

show absorptions at 301 nm, 313 nm, and 303 nm, respectively. Compared with the results of the pristine SWCNTs, a clear redshift of the characteristic SWCNT band is noticed in the results of the hybrid films, elaborating the strong interactions between the SWCNTs and polymers. Remarkably, the P2/SWCNTs and P3/SWCNTs nanocomposite films exhibit a larger redshift, indicating that these CPEs have stronger interactions with SWCNTs.

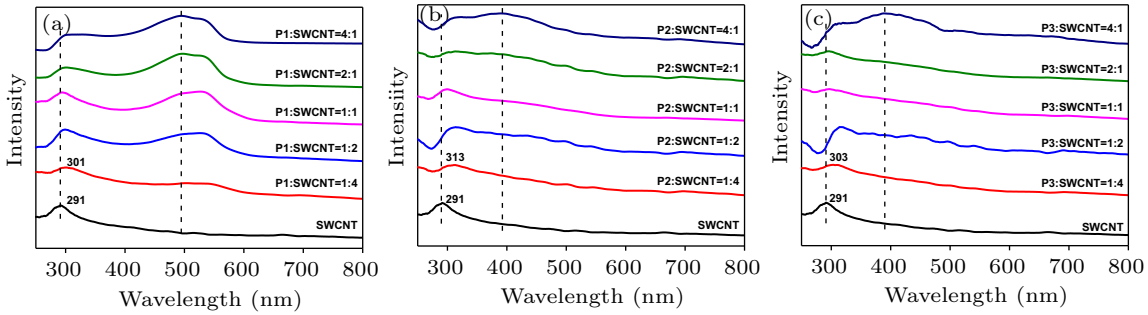


Fig. 3. UV–vis absorption spectra of nanocomposite films with different ratios. (a) P1/SWCNT, (b) P2/SWCNT, and (c) P3/SWCNT nanocomposites.

2.5. Raman spectroscopy

To further study the interactions between SWCNTs and polymers and the p-doping mechanism of P1, P2, and P3, SWCNTs and hybrid films are also characterized through Raman spectroscopy. As shown in Fig. 4, the SWCNTs present intensive G bands at approximately 1591 cm^{-1} and 1590 cm^{-1} originating from the in-plane rotational movement of chemical bonds from many couples of sp^2-hybridized C atoms.[21] However, the D bands at 1340 cm^{-1} are not observed, suggesting that the interaction does not introduce excessive defects in the SWCNTs. Pristine polymers show characteristic bands, namely, the C–S stretching vibration on the conjugated skeleton at 1343 cm^{-1}. The band at 1438 cm^{-1} originates from the C=C symmetrical stretching method of the benzene-alt-thiophene units.[22] In addition, the G band of SWCNTs from the polymer/SWCNT nanocomposite films redshifts in comparison to that of pristine SWCNTs. The Raman shift reflects the charge transfer from the SWCNTs to the polymers, which coincides with the p-type doping mechanism of SWCNTs.[23,24] Moreover, the P2/SWCNTs and P3/SWCNTs composite films exhibit a larger shift, which implies an increase in bond energy for sp^2 hybridized C atoms. This result is identical to the above mentioned results, which also explains why the CPEs have strong interaction with SWCNTs. Moreover, the Raman spectra can be used to observe the interaction between polymer and SWCNTs, a detectable blueshift indicates the strong π–π interaction between polymer chains and SWCNTs.[25] Therefore, P2 and P3 have stronger interaction with SWCNT than P1. Since P2 and P3 have similar segment structure, P2 and P3 have similar blueshift, the Reman spectra of the P2/SWCNT composite shift to a little bit higher wavenumber due to the ionic side chains of P2.

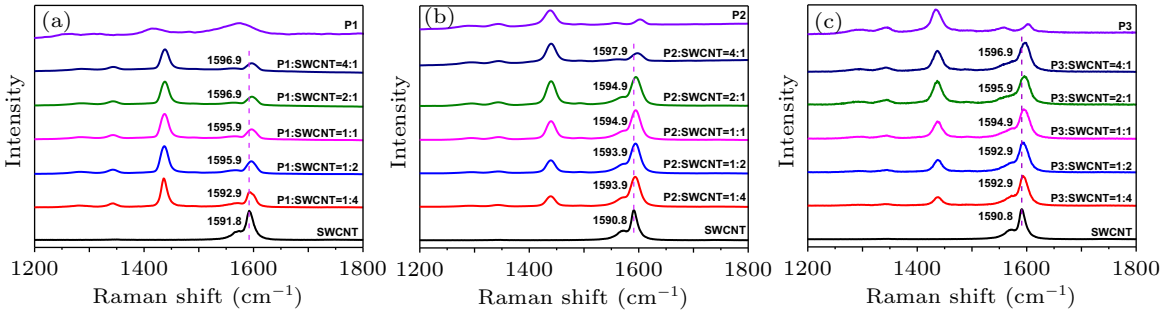


Fig. 4. Raman spectra of polymers, SWCNTs, and nanocomposite films with different ratios. (a) the P1, SWCNTs and P1/SWCNTs, (b) the P2, SWCNTs and P2/SWCNTs, and (c) the P3, SWCNTs and P3/SWCNTs.

2.6. X-ray photoelectron spectroscopy

To study the changes in the chemical bonding and chemical states of elements, the XPS is employed to characterize the materials. XPS of P2 and P2/SWCNT with 80 wt% SWCNTs is performed. As shown in Fig. 5(a), all the characteristic peaks (C 1s, O 1s, S 2p and Na 1s) of P2 and the P2/SWCNTs nanocomposites film are displayed. The Na 1s peak of P2 and the P2/SWCNTs nanocomposites film indicates the existence of ionic groups, further confirming that P2 is successfully composited with SWCNTs. In Fig. 5(b), the signal at approximately 285.2 eV can be attributed to C–O, and the peak at a higher binding energy of approximately 285.9 eV results from C–S. Moreover, the peak at approximately 284.8 eV originating from C–S, and the peak deconvolution of the C 1s of the P2/SWCNTs nanocomposite film (Fig. 5(c)) reveals a more important assembly at 284.5 eV, originating from the

C=C bond in the SWCNTs.[11,26] Regarding the S 2p spectrum, the original single S 2p doublet is logically divided into two doublets, involving S $2p^{3/2}$ and S $2p^{1/2}$, which is originate from the S element of the thiophene and sulfonate units, respectively (Figs. 5(d) and 5(e)). The decomposed S 2p doublet is noticed at binding energies of 164.38 eV and 165.48 eV, which originate from the S element in the thiophene units. The other S 2p doublets at 168.53 eV and 169.43 eV can be attributed to the S element in the sulfonate units.[27,28]

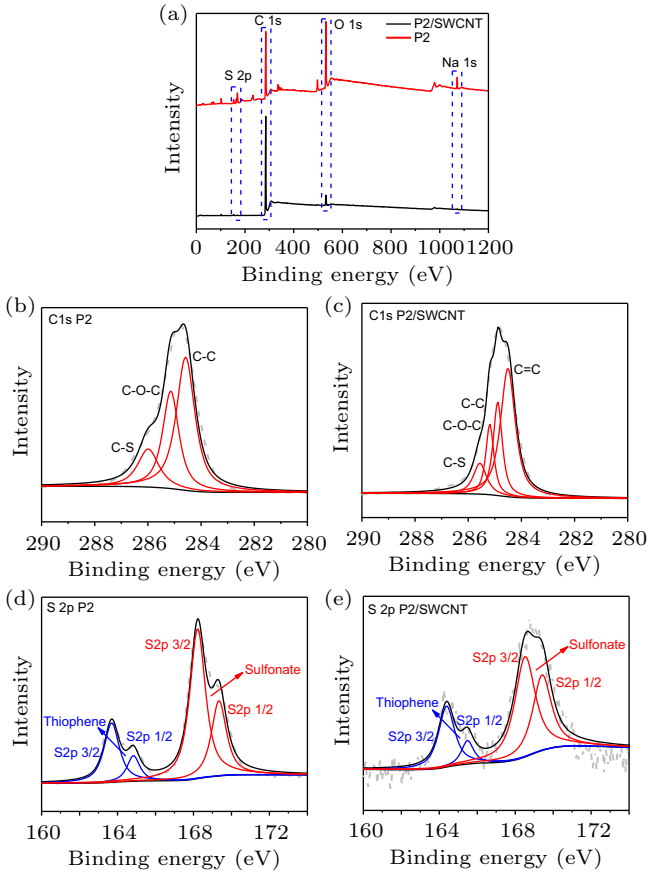


Fig. 5. (a) Deconvolution of the high-resolution XPS spectra of P2 and the P2/SWCNTs nanocomposite film with a mass ratio of 1:4, (b)–(c) C 1s peak of P2 and the P2/SWCNTs nanocomposites, (c)–(d) S 2p peak of P2 and P2/SWCNT nanocomposite film.

2.7. Thermoelectric properties

Regarding P1/SWCNTs, P2/SWCNTs, and P3/SWCNTs nanocomposite films, as presented in Figs. 6(a)–6(b), the electric conductivity and Seebeck coefficient with different mass ratios are measured at room temperature. The related power factor trends are summarized in Fig. 6(c). Clearly, the mixture of SWCNTs can greatly elevate the conductivity of P1, P2, and P3 (Fig. 6(a)). With increasing SWCNTs content, the conductivity becomes increasingly high because the three-dimensional conductive networks increase [29,30] Notably, the conductivities of the P2/SWCNTs and P3/SWCNTs composites with ionic side chains are higher than those of nonionic side chain P1/SWCNTs composites. As follows, the conductivities of the P1/SWCNTs, P2/SWCNTs, and P3/SWCNT nanocomposites with a mass ratio of 1:4 are 297 S·cm^{-1}, 3686 S·cm^{-1}, and 3803 S·cm^{-1}, respectively. Clearly, the electrical conductivities of the P2/SWCNTs and P3/SWCNTs nanocomposites with ionic side chains are nearly ten times the electrical conductivity of P1/SWCNTs. One reason for the improvement in the electrical conductivity owing to the strong π–π interaction between P2 and P3 and the SWCNTs, consistent with the above results, is that the stronger interaction leads to more three-dimensional conductive networks, and is more beneficial for carrier transport compared to the results with P1. Moreover, the orbital energy levels of P2 and P3 are different from those of P1 due to the ionic side chain, which is also beneficial to carrier transport. Furthermore, p-doping is usually the phenomenon in which electrons transfer from the highest occupied molecular orbital (HOMO) of the SWCNTs to the lowest occupied molecular orbital (LUMO) of the polymer. As shown above, the experimentally measured LUMO levels of P1 (−3.84 eV), P2 (−4.05 eV), and P3 (−4.3 eV), and the Fermi level of SWCNTs (−4.9 eV) reported in the literature are deeper than those of P1, P2, and P3.[31] However, the LUMO levels of P2 and P3 are more negative than that of P1, which can also promote the charge transport of P2/SWCNTs and P3/SWCNTs compared to P1/SWCNTs. These results are beneficial for improving the electrical conductivity of the P2/SWCNTs and P3/SWCNTs nanocomposites. Since the LUMO level of P3 is closest to the HOMO level of SWCNT, P3/SWCNT has the highest conductivity. The conductivity relationship can also be verified by the carrier mobility and carrier concentration shown in Table S2.

The Seebeck coefficients reveal that P1/SWCNTs, P2/SWCNTs, and P3/SWCNTs nanocomposites are all p-type thermoelectric materials, as shown in Fig. 6(b). The P1/SWCNTs nanocomposites have a larger Seebeck coefficient than P2/SWCNTs and P3/SWCNTs nanocomposites. The result can be explained through the relationship of conductivity and the Seebeck coefficient, whose values are all related to the carrier concentration as follows:

$$\sigma = neu, \tag{1}$$

$$S \propto \left(\frac{\pi}{3n}\right)^{\frac{2}{3}}. \tag{2}$$

In the light of Eqs. (1) and (2), the conductivity and Seebeck coefficient are negatively correlated. In other words, the P1/SWCNTs nanocomposites have a higher Seebeck coefficient, meaning a lower conductivity, and vice versa.

The power factor is calculated from the Seebeck coefficient and conductivity. Because the conductivity of P2/SWCNTs and P3/SWCNTs greatly improves and the Seebeck coefficient decreases less, the power factor of the P2/SWCNTs and P3/SWCNTs nanocomposites are larger than

that of P1/SWCNTs nanocomposites (Fig. 6(c)). In addition, when the SWCNT content increases, the trend of the power factor curve is similar to that of the electric conductivity, which also explains why the conductivity dominates the power factor. At room temperature, at a SWCNT content of 80 wt%, the power factors of P1/SWCNT, P2/SWCNT, and P3/SWCNT are 112 $\mu W{\cdot}m^{-1}{\cdot}K^{-2}$, 163 $\mu W{\cdot}m^{-1}{\cdot}K^{-2}$, and 151 $\mu W{\cdot}m^{-1}{\cdot}K^{-2}$, respectively.

To study the thermoelectric properties of the P1/SWCNTs, P2/SWCNT, and P3/SWCNT nanocomposites with 80 wt% SWCNT content at different temperatures, the conductivity, Seebeck coefficient and power factor are also tested. As presented in Figs. 6(d)–6(e), with increasing temperature, the conductivities of P2/SWCNTs and P3/SWCNTs gradually decrease above room temperature, which is contributed to a phenomenon of metallic conduction and temperature-induced de-doping effect, similar result has been reported by Li *et al.*[32] However, the Seebeck coefficients of P2/SWCNTs and P3/SWCNTs increase with increasing temperature, which can be explained by the heat-assisted jumping mechanism.[33,34] On the other hand, the Seebeck coefficient has an opposite dependence on the charge carrier concentration, temperature-induced de-doping effect will decrease the carrier concentration. As a result, the Seebeck coefficient of the P2/SWCNT and P3/SWCNT composites increases with the increasing temperature. However, the electrical conductivity of the P1/SWCNT composite has a lower value. At lower temperatures, the carrier concentration is thermally activated and is in accordance with Mott's variable-range-hopping (VRH) model, at higher temperatures, the carrier concentration is fully activated.[35] Therefore, the Seebeck coefficient of the P1/SWCNT composite changes oppositely in comparison with that of the P2/SWCNT and P3/SWCNT composites. As shown, the optimized power factors of P1/SWCNTs, P2/SWCNTs, and P3/SWCNTs are 87 $\mu W{\cdot}m^{-1}{\cdot}K^{-2}$, 327 $\mu W{\cdot}m^{-1}{\cdot}K^{-2}$, and 280 $\mu W{\cdot}m^{-1}{\cdot}K^{-2}$, respectively. Overall, at 460 K, the power factor of the P2/SWCNTs nanocomposites reaches a maximum of 327 $\mu W{\cdot}m^{-1}{\cdot}K^{-2}$, which is higher than that of P1/SWCNT nanocomposites with a maximum power factor of 87 $\mu W{\cdot}m^{-1}{\cdot}K^{-2}$ at 360 K. It is worth mentioning that, the ionic side chains of CPEs may obviously elevate the interactions between the CPEs and SWCNTs, thus enhancing the thermoelectric performance of the nanocomposites.

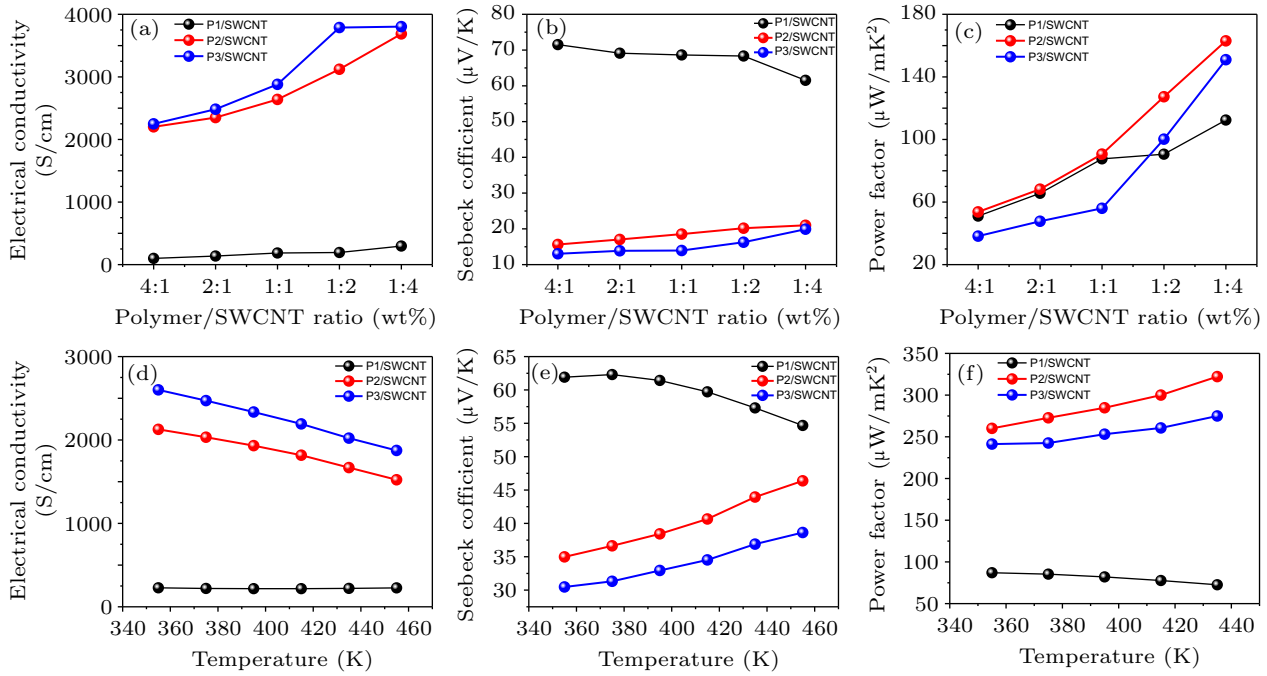


Fig. 6. Thermoelectric properties of nanocomposite films with different ratios at room temperature: (a) conductivities, (b) Seebeck coefficients, and (c) power factor. Thermoelectric properties of nanocomposite films with a mass ratio of 1:4 at different temperatures: (d) conductivities, (e) Seebeck coefficients, and (f) power factor.

2.8. Thermoelectric generator performance

To investigate their thermoelectric generator performance, three organic thermoelectric modules are fabricated using P1/SWCNTs, P2/SWCNTs and P3/SWCNTs nanocomposites with an 80% SWCNT content. Figure 7(a) shows the model diagram of the thermoelectric generator consisting of ten p-type thermoelectric films. The prepared p-type nanocomposites are connected to copper glue, and then silver glue is applied to the joint. The thermocouple is connected to the hot and cold ends to monitor the temperature difference ΔT ($\Delta T = T_{hot} - T_{cold}$). Figure 7(c) shows the theoretical (V_{TH})

and actual (V_{AC}) output voltage curves of the temperature difference (ΔT) of the P2/SWCNT nanocomposites. The actual voltages (V_{ACs}) are tested, and the theoretical voltages (V_{THs}) are calculated according to

$$V_{TH} = nST, \tag{3}$$

where n is the number of nanocomposite films, and S is the Seebeck coefficient of the p-type nanocomposite film. As presented in Fig. 7(c), V_{TH} and V_{AC} exhibit a very small difference, which is attributed to the carrier concentration decreased when thermally excited, because of the scarcity of carrier supplements of the n-type thermoelectric materials, leading to a small difference between V_{TH} and V_{AC}. Moreover, the V_{AC} linearly increases with the temperature difference, at $\Delta T = 70$ K, the V_{AC} reaches 27.3 mV.

Our thermoelectric modules are composed of P2/SWCNT composite films, whose total electrical resistance is approximately 120 Ω. As shown in Fig. 7(b), the measured current–voltage–power curves of the P2/SWCNTs composite films are presented at different ΔT values. The device generates a maximum output power of 1372 nW at $\Delta T = 70$ K. Figure S10 shows the current output–voltage output and power output curves for two other thermoelectric generators composed of P1/SWCNT and P3/SWCNT composite films at similar $\Delta T = 70$ K. The maximum output powers are 375 nW and 677 nW, respectively. Additionally, the calculated power density of thermoelectric modules composed of P2/SWCNT composite films is shown in Fig. 7(d), which gradually increases as ΔT increases. The maximum power density is 1.4 W·m^{-2} (cross-section) at $\Delta T = 70$ K. The thermoelectric modules containing ionic side-chain CPEs/SWCNTs nanocomposites achieve higher thermoelectric conversion efficiency than the non-CPEs/SWCNTs nanocomposites.

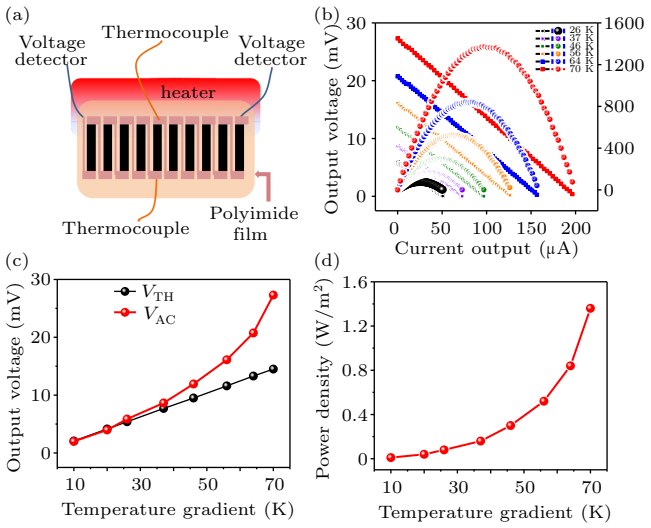


Fig. 7. (a) The model diagram of the thermoelectric generator, (b) the output voltage and power output curves from P2/SWCNT composite films at different ΔT, (c) the output voltage curves of V_{TH} and V_{AC} at different ΔT, and (d) the calculated power density at different ΔT.

3. Conclusion

We synthesize and characterize three types of polymers (P1, P2, and P3) with identical conjugated skeletons but bearing different side chains. The ionic side chains of CPEs may obviously elevate the interactions between the CPEs and SWCNTs, thus enhancing the thermoelectric performance of the nanocomposites. Therefore, the P2/SWCNTs and P3/SWCNTs nanocomposites with an 80% SWCNTs content present high conductivities of 3586 S·cm^{-1} and 3803 S·cm^{-1}, respectively, which are ten times that of P1/SWCNTs (297 S·cm^{-1}). Because the conductivity of P2/SWCNTs is greatly improved and the Seebeck coefficient decreases less, the power factor of P2/SWCNTs (164 μW·m^{-1}·K^{-2}) is larger that of P1/SWCNTs (112 μW·m^{-1}·K^{-2}). Consequently, the thermoelectric module containing CPEs composite films (P2/SWCNTs) achieves a high output voltage of 27.3 mV, output power of 1.37 μW, and power density of 1.4 W·m^{-2} (cross-section) at $\Delta T = 70$ K, which is three times higher than the thermoelectric generator containing non-CPEs composite films (P1/SWCNT 0.37 μW). This method of constructing CPEs/SWCNTs composites can be applied in the production of thermoelectric materials and devices.

Acknowledgements

This work was supported by the National Natural Science Foundation of China (Grant Nos. 51803126 and 21704065) and the Natural Science Foundation of Guangdong Province, China (Grant No. 2018A0303130157). We thank the Instrumental Analysis Centre of Shenzhen University for analytical support.

References

[1] Fan F R, Tang W and Wang Z L 2016 *Adv. Mater.* **28** 4283
[2] Wang Z L and Wu W 2012 *Angew. Chem. Int. Ed.* **51** 11700
[3] Bubnova O, Khan Z U, Malti A, Braun S, Fahlman M, Berggren M and Crispin X 2011 *Nat. Mater.* **10** 429
[4] Chen Y, Zhao Y and Liang Z 2015 *Energy Environ. Sci.* **8** 401
[5] Yu C, Choi K, Yin L and Grunlan J C 2011 *Acs Nano* **5** 7885
[6] Li C, Jiang F, Liu C, Wang W, Li X, Wang T and Xu J 2017 *Chem. Eng. J.* **320** 201
[7] Niemela J P, Karttunen A J and Karppinen M 2015 *J. Mater. Chem. C* **3** 10349
[8] Fan W, Zhang Y, Guo C Y and Chen G 2019 *Compos. Sci. Technol.* **183** 107794
[9] Lan X, Wang T, Liu C, Liu P, Xu J, Liu X, Du Y and Jiang F 2019 *Compos. Sci. Technol.* **182** 107767
[10] Zhou Y, Yin X, Liu Y, Zhou X, Wan T, Wang S, Gao C and Wang L 2019 *ACS Sustain. Chem. Eng.* **7** 11832
[11] Hao L, Kang J, Shi J, Xu J, Cao J, Wang L, Liu Y and Pan C 2020 *Compos. Sci. Technol.* **199** 108359
[12] Niu R, Pan C, Chen Z, Wang L and Wang L 2020 *Chem. Eng. J.* **381** 122650
[13] Cui Q and Bazar G C 2018 *Acc. Chem. Res.* **51** 202
[14] Mai C K, Schlitz R A, Su G M, Spitzer D, Wang X, Fronk S L, Cahill D G, Chabinyc M L and Bazan G C 2014 *J. Am. Chem. Soc.* **136** 13478

[15] Mai C K, Arai T, Liu X, Fronk S L, Su G M, Segalman R A, Chabinyc M L and Bazan G C 2015 *Chem. Commun.* **51** 17607

[16] Mai C K, Russ B, Fronk S L, Hu N, Chan-Park M B, Urban J J, Segalman R A, Chabinyc M L and Bazan G C 2015 *Energy Environ. Sci.* **8** 2341

[17] Li Y, Mai C K, Hung P, Liu X, Thuc-Quyen N, Bazan G C and Chan-Park M B 2014 *Adv. Mater.* **26** 4697

[18] Wang L, Pan C, Liang A, Zhou X, Zhou W, Wan T and Wang L 2017 *Polym. Chem.* **8** 4644

[19] Zhou X, Pan C, Liang A, Wang L and Wong W Y 2017 *Compos. Sci. Technol.* **145** 40

[20] Liu T, Shinohara A, Tan G, Pan C and Wang L 2019 *Macromol. Mater. Eng.* **304** 1800730

[21] Ritter U, Scharff P, Siegmund C, Dmytrenko O P, Kulish N P, Prylutskyy Y I, Belyi N M, Gubanov V A, Komarova L I, Lizunova S V, Poroshin V G, Shlapatskaya V V and Bernas H 2006 *Carbon* **44** 2694

[22] Wang Y Y, Cai K F, Shen S and Yao X 2015 *Synth. Met.* **209** 480

[23] Wang H, Hsu J H, Yi S I, Kim S L, Choi K, Yang G and Yu C 2015 *Adv. Mater.* **27** 6855

[24] An C J, Kang Y H, Song H, Jeong Y and Cho S Y 2017 *J. Mater. Chem. A* **5** 15631

[25] Zhou H, Li X, Gao C, Yang F, Ye X, Liu Y and Wang L 2021 *Compos. Sci. Technol.* **201** 108518

[26] Cho S, Seo J H, Park S H, Beaupre S, Leclerc M and Heeger A J 2010 *Adv. Mater.* **22** 1253

[27] Zhou H, Gao C, Liu T, Pan C and Wang L 2020 *J. Mater. Chem. C* **8** 7096

[28] Karlsson R H, Herland A, Hamedi M, Wigenius J A, Aslund A, Liu X, Fahlman M, Inganas O and Konradsson P 2009 *Chem. Mater.* **21** 1815

[29] Tan J, Huang H, Wang D, Qin S, Xiao X, Chen Z, Liu D and Wang L 2020 *J. Mater. Chem. C* **8** 4827

[30] Tan J, Chen Z, Wang D, Qin S, Xiao X, Xie D, Liu D and Wang L 2019 *J. Mater. Chem. A* **7** 24982

[31] Kim S L, Choi K, Tazebay A and Yu C 2014 *Acs Nano* **8** 2377

[32] Li B, Mao Y, Mao X, Liu Y, Li X, Zhou Y, Wang S, Yang F, Gao C and Wang L 2020 *ACS Appl. Energy Mater.* **3** 11947

[33] Zhao W, Fan S, Xiao N, Liu D, Tay Y Y, Yu C, Sim D, Hng H H, Zhang Q, Boey F, Ma J, Zhao X, Zhang H and Yan Q 2012 *Energy Environ. Sci.* **5** 5364

[34] Wan T, Yin X, Pan C, Liu D, Zhou X, Gao C, Wong W Y and Wang L 2019 *Polymers* **11** 593

[35] Zhang Q, Sun Y, Xu W and Zhu D 2012 *Energy Environ. Sci.* **5** 9639